Nano-oxide-layer insertion and specular effects in spin valves: Experiment and theory

L. Wang,[1,*] J. J. Qiu,[1] W. J. McMahon,[1] K. B. Li,[1] and Y. H. Wu[1,2,†]
[1]*Nano Spinelectronics, Data Storage Institute, DSI Building, 5 Engineering Drive 1, Singapore 117608, Singapore*
[2]*Department of Electrical and Computer Engineering, National University of Singapore, 10 Kent Ridge Crescent, Singapore 119260, Singapore*

(Received 30 September 2003; published 3 June 2004)

We report a systematic study of NOL (nano-oxide-layer) insertion and specular effects on the giant magnetoresistance (GMR) of single, synthetic, and dual spin valves, using a semiclassical Boltzmann theory. It is confirmed that the GMR ratio is enhanced by NOL insertion inside the pinned layer or after the free layer. The enhancements are primarily due to the contribution of the majority carriers. The NOL insertions inside the inactive layers of spin valves such as the seed, under, and capping layers reduce the GMR ratio. Though introducing a NOL before or after the Cu spacer would, in principle, significantly suppress the GMR ratio due to the blocking effect or the average effect of different spin channels, large positive or negative (inverse) GMR is found by assuming spin-dependent NOL specular reflections. We have also demonstrated that specular reflection, even beyond a capping layer, may result in reduction of GMR. Upon appropriate NOL insertion, the amplitude of curve of GMR versus thickness of individual layer of spin valves may be generally enhanced, but the shape may change, depending on whether the distance of the NOL to the layer is small or large (distance effect). Finally, it is found that most results obtained for the single realistic spin valves are applicable to synthetic and dual spin valves.

DOI: 10.1103/PhysRevB.69.214402 PACS number(s): 75.70.Cn, 75.47.De, 72.10.−d

I. INTRODUCTION

Magnetoresistance refers to the change of electrical resistance for a system in the presence of an external magnetic field. Giant magnetoresistance (GMR), with a large change in resistance, occurs in magnetic multilayers when the magnetizations of the ferromagnetic layers are reoriented relative to one another under the application of an external magnetic field. The discovery of GMR (Refs. 1 and 2) not only has had a vast impact on the present and future of the recording and computer industry (see, e.g., Ref. 3), but also has stimulated significant progress in the transport theory in magnetic layered structures.[4]

Although the GMR in multilayers may be quite large, the corresponding applied magnetic field also needs to be large. The data storage industry requires sensitivity to small magnetic fields, thus the invention of the spin valve (SV) (Refs. 5–8) becomes important because of their sensitivity to small magnetic fields. The critical region of a spin valve consists of two ferromagnetic layers, separated by a nonmagnetic spacer. The magnetization of one ferromagnetic layer is pinned by exchange coupling with an adjacent antiferromagnetic (AFM) layer, whereas the magnetization of the other ferromagnetic layer is free to rotate with the applied magnetic field.

The GMR phenomena may be attributed to spin-dependent scattering occurring in the bulk of the ferromagnetic layers, at the ferromagnetic/nonmagnetic interfaces, and/or the surfaces (see, e.g., Ref. 9). In this paper, particular attention is given to one kind of scattering, i.e., specular scattering (reflection). In this case, specular reflection occurs when the component of an electron's wave vector parallel to the interface remains unchanged, and the direction of electron spin is conserved. The effect of such a reflection is to extend the mean free path (MFP) of majority spin-polarized electrons. This effectively increases the number of electrons within the critical region of a spin valve or the number of multilayers seen by an electron, thus improving the GMR of spin valves. The cause of GMR enhancement of the following reports has been attributed to specular reflection: (i) inserting nano-oxide layers (NOL) into spin valves,[10–15] (ii) depositing noble metals on top of spin valves,[16–18] (iii) using NiO and α-Fe_2O_3 oxides as the AFM layer,[19–21] and (iv) using oxygen as a surfactant during the film deposition.[22,23]

Analyses of specular reflection are mainly based on the pioneering Fuchs and Sondheimer (FS) theory[24,25] that uses the Boltzmann transport equation; this was initially applied to the resistivity of thin films, and extended to multilayers by Carcia and Suna.[26] Camley and Barnaś (CB) later applied this semiclassical theory to magnetic multilayers to study GMR by taking into account spin-dependent transport of electrons.[27,28] Hood and Falicov (HF)[29] further emphasized scattering at interfaces. The CB and HF theories[27–29] have been extensively used to treat specular reflection in GMR.[19,30–33] Alternatively, specular reflection can be dealt with quantum mechanically,[34–36] where the main starting point is the Kubo formalism.[37] However, the focus of these semiclassical and quantum mechanical works on the specular reflection is only on certain positions in spin valves. The same conclusion also holds for the semiclassical study of NOL specular reflections.[38–40] Hence, a systematic theoretical study of NOL insertion positions (specular reflection) is currently still lacking and thus no comparison has been made between the corresponding theory and experiment. In view of this and in light of the fact that nano-oxide spin valves are one of the key components in the cutting-edge HDD (hard disk drive) technology (over 100 Gb/in.^{2}),[41] developing a model that systematically addresses the oxide insertion and

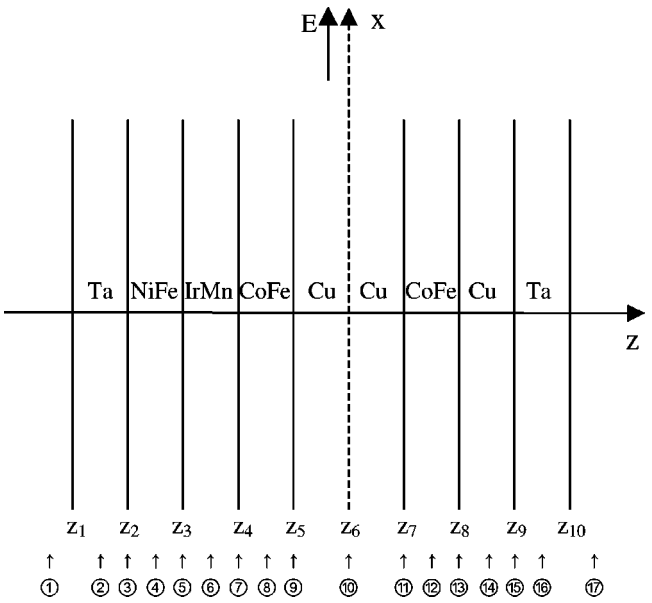

FIG. 1. Schematic diagram of the layered structure of a bottom spin valve. The z axis is normal to the layers. z_i is the position of surfaces and interfaces. The x axis, located at $z_{i_0}=0$, splits the Cu spacer into two parts. The electric field E is applied parallel to the x axis. The insertion positions of the nano-oxide layer are the surfaces, interfaces, and midpoints of the layers.

specular effects is both interesting and necessary.

The rest of this paper is organized as follows: In Sec. II, a brief description of our experiments is given. A semiclassical model is presented in detail in Sec. III. In Sec. IV, we focus on single spin valves. Results and discussion are also presented for synthetic and dual spin valves before concluding.

II. EXPERIMENT

A series of spin valve samples were deposited on 1 in. $\times 1$ in. Si(100) wafers coated with 1 μm thick thermally oxidized SiO_2 layer by using an ultrahigh-vacuum (UHV) sputtering system under a base pressure of 5×10^{-10} Torr. The basic structure of the spin valves is Ta (30)/ NiFe (20)/ IrMn (60)/ CoFe (30)/ Cu (24)/ CoFe (25)/ Cu (10)/ Ta (30) (thicknesses are in Å). The nano-oxide layers were formed by exposing the fresh metal surfaces to pure oxygen atmosphere in a separated load-lock UHV chamber (without breaking the vacuum). All samples were grown at room temperature and under a magnetic field of 100 Oe applied to induce the easy axes of magnetic layers during deposition. The unidirectional anisotropy was further set by magnetically annealing in a commercial oven for 2 h at 235 °C and at a field of 1 T. The room-temperature magnetoresistance was measured using a four-probe setup.

III. THEORY

Spin valves usually operate in two modes: CIP (current in plane) and CPP (current perpendicular to plane). Oxides may affect the properties of the CPP spin valve[42] (and tunneling magnetoresistance,[43] which is similar to the CPP configuration). Here, our attention is confined to the CIP mode. Shown schematically in Fig. 1 is our modeling prototype, a bottom spin valve (BSV). The structure of the BSV is organized from left to right as: (1) seed layer Ta, (2) under layer NiFe, (3) antiferromagnetic layer IrMn, (4) ferromagnetic pinned layer CoFe, (5) spacer layer Cu, (6) spacer layer Cu, (7) ferromagnetic free layer CoFe, (8) filter layer Cu, and (9) capping layer Ta. The seed layer is deposited on the Si/SiO_2 substrate. The under layer is to ensure the desired (111) crystal structure of the AFM layer. A fictitious spin quantization axis is placed in the spacer layer, corresponding to an arbitrary position where the spin directions (up or down) are changed with certain probabilities determined by the angle between the magnetization directions of the pinned and free layers. The Cu filter layer usually increases the GMR effect by enhancing spin-dependent transport.

The electric current density in each layer is determined by the specific distribution functions for electrons with spin σ ($\uparrow$ or $\downarrow$) in that layer. Because of the symmetry in geometry within the film plane and the infinite boundaries in the x and y directions, this distribution of electrons is a function of velocity $\boldsymbol{v}$ and only the z component of the position vector. In this case, the linearized Boltzmann equation in the relaxation time approximation is

$$\frac{\partial g_{i\sigma}}{\partial z}+\frac{g_{i\sigma}}{\tau_{i\sigma}v_z}=\frac{eE}{m_{i\sigma}v_z}\frac{\partial f_0(\boldsymbol{v})}{\partial v_x}, \tag{1}$$

where $\tau_{i\sigma}$ is the relaxation time of electrons with spin σ in layer i ($i=1,2,\ldots,n$, where n is the number of layers. For the prototype BSV in Fig. 1, $n=9$). $m_{i\sigma}$ is the effective mass of electrons and e is the electron charge. $g_{i\sigma}(z,\boldsymbol{v})$ is the deviation from the equilibrium distribution function $f_0(\boldsymbol{v})$, namely, $g_{i\sigma}(z,\boldsymbol{v})=f_{i\sigma}(z,\boldsymbol{v})-f_0(\boldsymbol{v})$.

The general form of the solution to Eq. (1) is

$$g^{\pm}_{i\sigma}(z,\boldsymbol{v})=\frac{eE\tau_{i\sigma}}{m_{i\sigma}}\frac{\partial f_0(\boldsymbol{v})}{\partial v_x}\left[1+F^{\pm}_{i\sigma}(\boldsymbol{v})\exp\left(\frac{\mp z}{\tau_{i\sigma}|v_z|}\right)\right], \tag{2}$$

where $g_{i\sigma}(z,\boldsymbol{v})$ has been divided into two parts: $g^{+}_{i\sigma}(z,\boldsymbol{v})$ if $v_z\geqslant 0$ and $g^{-}_{i\sigma}(z,\boldsymbol{v})$ if $v_z<0$. The $4n$ unknown parameters $F^{\pm}_{i\sigma}(\boldsymbol{v})$ should be determined by appropriate boundary and interfacial conditions.

Denoting the index of the position of the x axis as i_0 ($i_0=6$ in Fig. 1), the surface and interface conditions[27] can be cast as follows:

$$g^{+}_{1\sigma}=p_{l\sigma}g^{-}_{1\sigma}, \tag{3a}$$

$$g^{-}_{i\sigma}=S_{i+1,i,i,\sigma}T_{i+1,i,\sigma}g^{-}_{i+1,\sigma}+S_{i,i+1,i,\sigma}R_{i,i+1,\sigma}g^{+}_{i\sigma} \tag{3b}$$

$$g^{+}_{i\sigma}=S_{i-1,i,i,\sigma}T_{i-1,i,\sigma}g^{+}_{i-1,\sigma}+S_{i,i-1,i,\sigma}R_{i,i-1,\sigma}g^{-}_{i\sigma} \tag{3c}$$

$$g^{-}_{i_0-1,\sigma}=\cos^2(\theta/2)g^{-}_{i_0,\sigma}+\sin^2(\theta/2)g^{-}_{i_0,-\sigma}, \tag{3d}$$

$$g^{+}_{i_0,\sigma}=\cos^2(\theta/2)g^{+}_{i_0-1,\sigma}+\sin^2(\theta/2)g^{+}_{i_0-1,-\sigma}, \tag{3e}$$

$$g^{-}_{n\sigma}=p_{r\sigma}g^{+}_{n\sigma}. \tag{3f}$$

Values of the i index in Eqs. (3b) and (3c) are $i=1,2,\ldots,i_0-2,i_0,\ldots,n-1$ and $i=2,3,\ldots,i_0-1,i_0+2,\ldots,n$, respectively. The Fuchs specularity factors, $p_{l\sigma}$ [Eq. (3a)] and $p_{r\sigma}$ [Eq. (3f)] for the left and right surfaces, take values between 0 (completely diffusive scattering) and 1 (completely specular reflection) and provide a measure of the surface roughness and barrier height. The notation used for the transmission T and the reflection R coefficients is defined. $T_{i,j,\sigma}\equiv$ probability for an electron of spin σ in layer i to be transmitted (refracted) into layer j. $R_{k,l,\sigma}\equiv$ probability for an electron of spin σ in layer k with a velocity directed towards layer l to be reflected back into layer k. $S_{i,j,l,\sigma}$, which vary between 0 and 1, are factors that indicate the degree of potential scattering at each of the interfaces (i,j) for a spin σ electron arriving from layer i and being scattered into the layer l. The scattering follows the reflection-refraction laws when $S=1$ and is completely diffusive when $S=0$. θ in Eqs. (3d) and (3e) is the angle between the magnetization directions of the pinned and free layers. Note that the angular dependence of the surface scattering parameters,[44–46] the transmission coefficients,[29,47] the reflection coefficients,[29] and the interface scattering parameter[48] has been studied. In our simulations to focus on the oxide effects, we treat them as angle independent.

Substituting Eq. (2) into Eq. (3) leads to the following set of equations:

$$c_{1,1,\sigma}F^{+}_{1\sigma}-\frac{p_{l\sigma}}{c_{1,1,\sigma}}F^{-}_{1\sigma}=p_{l\sigma}-1, \tag{4a}$$

$$\begin{aligned}&-S_{i,i+1,i,\sigma}R_{i,i+1,\sigma}c_{i+1,i,\sigma}F^{+}_{i\sigma}+\frac{1}{c_{i+1,i,\sigma}}F^{-}_{i\sigma}\\&-\frac{S_{i+1,i,i,\sigma}T_{i+1,i,\sigma}y_{i+1,i,\sigma}}{c_{i+1,i+1,\sigma}}F^{-}_{i+1,\sigma}\\&=S_{i,i+1,i,\sigma}R_{i,i+1,\sigma}+S_{i+1,i,i,\sigma}T_{i+1,i,\sigma}y_{i+1,i,\sigma}-1,\end{aligned} \tag{4b}$$

$$\begin{aligned}&-S_{i-1,i,i,\sigma}T_{i-1,i,\sigma}y_{i-1,i,\sigma}c_{i,i-1,\sigma}F^{+}_{i-1,\sigma}+c_{i,i,\sigma}F^{+}_{i\sigma}\\&-\frac{S_{i,i-1,i,\sigma}R_{i,i-1,\sigma}}{c_{i,i,\sigma}}F^{-}_{i\sigma}\\&=S_{i,i-1,i,\sigma}R_{i,i-1,\sigma}+S_{i-1,i,i,\sigma}T_{i-1,i,\sigma}y_{i-1,i,\sigma}-1,\end{aligned} \tag{4c}$$

$$F^{-}_{i_0-1,\sigma}=\cos^2(\theta/2)F^{-}_{i_0,\sigma}+\sin^2(\theta/2)F^{-}_{i_0,-\sigma}, \tag{4d}$$

$$F^{+}_{i_0,\sigma}=\cos^2(\theta/2)F^{+}_{i_0-1,\sigma}+\sin^2(\theta/2)F^{+}_{i_0-1,-\sigma}, \tag{4e}$$

$$\begin{aligned}&-\frac{S_{i,i+1,i,\sigma}R_{i,i+1,\sigma}}{c_{i+1,i,\sigma}}F^{+}_{i\sigma}+c_{i+1,i,\sigma}F^{-}_{i\sigma}\\&-S_{i+1,i,i,\sigma}T_{i+1,i,\sigma}y_{i+1,i,\sigma}c_{i+1,i+1,\sigma}F^{-}_{i+1,\sigma}\\&=S_{i,i+1,i,\sigma}R_{i,i+1,\sigma}+S_{i+1,i,i,\sigma}T_{i+1,i,\sigma}y_{i+1,i,\sigma}-1,\end{aligned} \tag{4f}$$

$$\begin{aligned}&-\frac{S_{i-1,i,i,\sigma}T_{i-1,i,\sigma}y_{i-1,i,\sigma}}{c_{i,i-1,\sigma}}F^{+}_{i-1,\sigma}+\frac{1}{c_{i,i,\sigma}}F^{+}_{i\sigma}\\&-S_{i,i-1,i,\sigma}R_{i,i-1,\sigma}c_{i,i,\sigma}F^{-}_{i\sigma}\\&=S_{i,i-1,i,\sigma}R_{i,i-1,\sigma}+S_{i-1,i,i,\sigma}T_{i-1,i,\sigma}y_{i-1,i,\sigma}-1,\end{aligned} \tag{4g}$$

$$c_{n+1,n,\sigma}F^{-}_{n\sigma}-\frac{p_{r\sigma}}{c_{n+1,n,\sigma}}F^{+}_{n\sigma}=p_{r\sigma}-1. \tag{4h}$$

The values of the i index in Eqs. (4b), (4c), (4f), and (4g) run from $1\rightarrow i_0-2$, $2\rightarrow i_0-1$, $i_0\rightarrow n-1$, and $i_0+1\rightarrow n$, respectively. The c coefficients in the above equations are introduced as follows:

$$c_{j,k,\sigma}=\exp\left(\frac{|z_j|}{\lambda_{k\sigma}|\cos\beta|}\right), \tag{5}$$

where β is the angle between the velocity and the z axis and $\lambda_{k\sigma}$ is the mean free path defined by $\lambda_{k\sigma}=v_{Fk\sigma}\tau_{k\sigma}$, with $v_{Fk\sigma}$ being the Fermi velocity. The parameters $y_{i,j,\sigma}$ account for the difference in the electronic properties of both the magnetic and nonmagnetic layers and are defined as

$$y_{i,j,\sigma}=\frac{\lambda_{i\sigma}/m_{i\sigma}v_{Fi\sigma}}{\lambda_{j\sigma}/m_{j\sigma}v_{Fj\sigma}}, \tag{6}$$

with i and j denoting the indices of adjacent two layers.

Solutions of the linear system of Eq. (4) yield the values of the $F^{\pm}_{i\sigma}(\boldsymbol{v})$ parameters and consequently, the perturbation of the electron distribution. The current density along the electric field in each layer i for electrons with spin σ is given by

$$J_{xi\sigma}(z)=e(m_{i\sigma}/h)^3\int v_x g_{i\sigma}(z,\boldsymbol{v})d^3\boldsymbol{v}, \tag{7}$$

where h is Planck's constant. The corresponding local conductivity is (the symbol of spin, σ, is here also used for conductivity)

$$\sigma_{xi\sigma}(z)=J_{xi\sigma}(z)/E. \tag{8}$$

The overall conductivity σ of the layered structure is

$$\sigma=\frac{1}{d}\sum_{i=1}^{n}\sum_{\sigma=\uparrow,\downarrow}\int\sigma_{xi\sigma}(z)dz, \tag{9}$$

where d is the total thickness of the SV structure. The sheet resistance R_s of the entire structure is then

$$R_s=\frac{1}{\sigma d} \tag{10}$$

$$=1\Big/\sum_{i=1}^{n}\sum_{\sigma=\uparrow,\downarrow}\int\sigma_{xi\sigma}(z)dz. \tag{11}$$

R_s is a function of θ. $R_s(\theta=0)$ and $R_s(\theta=\pi)$ are the sheet resistances corresponding to the parallel and antiparallel

alignments of the magnetizations of the free and pinned layers. Denoting $R_s(\theta=0)$ and $R_s(\theta=\pi)$ as $R_s^{\uparrow\uparrow}$ and $R_s^{\uparrow\downarrow}$, the GMR ratio is defined as

$$\mathrm{GMR}(\%)=\frac{R_s^{\uparrow\downarrow}-R_s^{\uparrow\uparrow}}{R_s^{\uparrow\uparrow}}\times 100\%. \tag{12}$$

IV. RESULTS AND DISCUSSION

We begin this section by providing typical values of the parameters used in our simulations. The thickness of each layer of the spin valve follows our experimental settings: Ta (30)/ NiFe (20)/ IrMn (60)/ CoFe (30)/ Cu (24)/ CoFe (25)/ Cu (10)/ Ta (30), where the unit is in Å. Values of the mean free paths used are similar to those in Ref. 39: $\lambda_{\mathrm{NiFe}}^{\uparrow}=60$ Å, $\lambda_{\mathrm{NiFe}}^{\downarrow}=6$ Å, $\lambda_{\mathrm{CoFe}}^{\uparrow}=90$ Å, $\lambda_{\mathrm{CoFe}}^{\downarrow}=6$ Å, $\lambda_{\mathrm{Cu}}^{\uparrow\downarrow}=300$ Å, and $\lambda_{\mathrm{Ta}}^{\uparrow\downarrow}=6$ Å. We take $\lambda_{\mathrm{IrMn}}^{\uparrow\downarrow}=3$ Å, which is close to the value of $\lambda_{\mathrm{PtMn}}^{\uparrow\downarrow}=2$ Å as used in Ref. 32. The NOL insertion positions are in the middle of each layer, inside each interface, and outside the outer surfaces (see Fig. 1). Here, the corresponding NOL's are treated in a unified manner for convenience although the true oxides may be different from each other. Typical values of the NOL mean free path and the NOL thickness are chosen as $\lambda_{\mathrm{NOL}}^{\uparrow\downarrow}=20$ Å and $d_{\mathrm{NOL}}=15$ Å, but the qualitative nature of the results is not sensitive to the choice of λ_{NOL} or d_{NOL} provided that other parameters are fixed. The left and right specular factors, $p_{l\sigma}$ and $p_{r\sigma}$, are set at 0 and 1, respectively. These choices are reasonable since the specularity of the left Ta surface should be smaller than that of the right Ta surface due to the oxidation of the right surface caused by exposure to air. We take the transmission and reflection parameters as: $T=1$,[32,39] $R=0$,[27,28,30,32,39] $T_{\mathrm{NOL}}=0.1$, and $R_{\mathrm{NOL}}=0.8$ (which is close to the values of 0.81 and 0.85 in Refs. 40 and 38, respectively). The S parameters are chosen to be 1 for all layers. In the current parametrization scheme, S, T, and R are spin independent and the mean free paths in the ferromagnetic layers are spin dependent. These choices indicate bulk scattering only, which is our main concern in this paper. By assuming spin-dependent S, T, and R, properties of interface scattering can be investigated: to account for some interface spin asymmetry effects, spin-dependent R_{NOL} (Fig. 6) and S (Fig. 7) have been assumed. Our other preliminary results seem to indicate that upon interfacial spin-dependent scattering, some thickness dependences of GMR will be affected while the qualitative trends of GMR versus the NOL positions in single, synthetic, and dual spin valves will roughly remain the same. A full exploration of this important issue deserves a systematic study and a separate space.[49] Note that for simplicity the effective mass[29] and the Fermi velocity[50,51] are assumed constant. We take $m_{i\sigma}=4$ and $v_{Fi\sigma}=0.25$, both in atomic units. Our parametrization scheme here is simple and serves the dual role of allowing extensive investigation of complex spin valve systems at the same time as giving qualitative agreement with our experiments. Note that it is difficult to theoretically obtain unique and unambiguous settings of the parameters for realistic spin valves and the actual values of the parameters may also be process dependent.

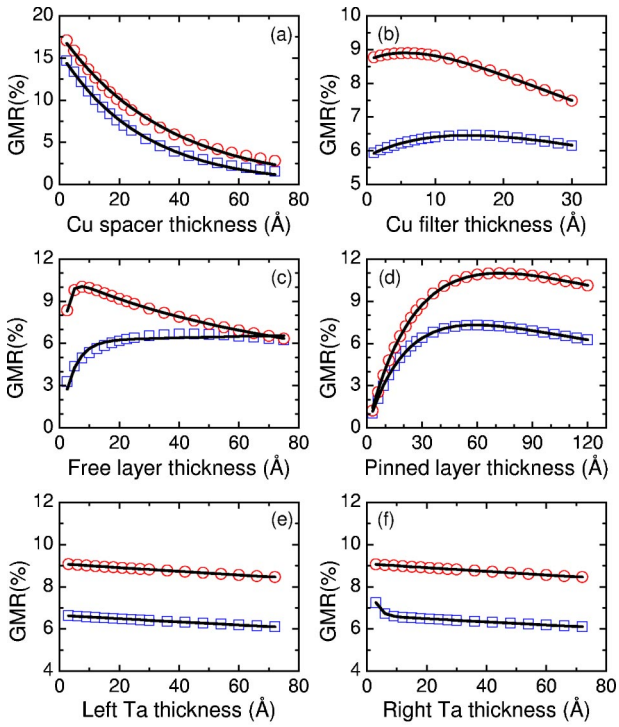

FIG. 2. (Color online) GMR ratios as a function of thickness of different layers of a bottom spin filter spin valve (see Fig. 1) with (○) and without the oxide layer (□) inserted at the filter layer/ capping layer interface. The solid curves are fits to the calculated data.

A. Thickness dependences of GMR

In Fig. 2, we present various thickness dependences of GMR ratios with (circles) and without (squares) the insertion of an oxide layer at position 15 after the Cu filter layer (see Fig. 1). The purpose of doing so is twofold. Our first goal is to verify the formalism presented in the preceding section by comparing the calculated thickness dependences of GMR with those in existing literature. The second aim is to show that the problem itself is interesting and worthy of detailed discussion. It can be seen in Fig. 2 that the GMR ratios in all cases are enhanced by the NOL insertion, compared to the corresponding situations without insertion. These overall GMR enhancements are ascribed to the NOL large specular reflection which results in more carriers experiencing spin-dependent transport.

The dependences of GMR on the thickness of the Cu spacer before and after the NOL insertion are quite similar to each other [see Fig. 2(a)] and are consistent with the calculated trends for similar studies in top spin valves (see Fig. 1 in Ref. 38 and Fig. 2 in Ref. 39, respectively). In fact, it is found that the calculated GMR ratios can be well fitted by exponential decay. This fact is consistent with the established pioneering experiment by Dieny *et al.*[7]

Figure 2(b) shows that a plateau of maximum GMR occurs in the range 10–20 Å of the Cu filter thickness for the non-insertion case. Our experimental optimized value of 11 Å falls in this domain. Upon the NOL insertion, the maxi-

mum is shifted to thinner filter thickness and the trend of GMR against the filter thickness is in qualitative agreement with Ref. 40.

The shift feature is also observed in Fig. 2(c) for the free layer case. Similar shifts have been found in the cases such as the transformation from trilayer to multilayer[52,53] and the increase of interface[19,51] or surface[4,28,54] specular reflections. Such kinds of shifts may provide valuable references for practical designs of spin valves. The qualitative trend, first increase and then decrease, of GMR against free layer thickness in Fig. 2(c) is also consistent with some reported work.[31,40,55]

As in Fig. 2(a), resemblances between the insertion and non-insertion cases are also observed in Figs. 2(d) and 2(e). It is found from Fig. 2(d) that GMR ratios still increase at very large thickness of the pinned layer at about 50 Å. This increasing trend is fairly consistent with the work of Dieny *et al.*[32] (see the non-specular case, i.e., $R=0$, in Fig. 4 in the reference).

Figure 2(e) shows that the plots of GMR versus the thickness of the left Ta layer (d_{Ta^l}) exhibit linear behaviors. Upon the NOL insertion, a linear decrease is also observed with the thickness of the right Ta layer (d_{Ta^r}), as shown in Fig. 2(f). However, for the non-NOL insertion case a steep drop occurs at short capping thickness followed by a linear behavior. Similar fast drops have been experimentally observed by Egelhoff *et al.*[16]

There have been a few analytical descriptions of GMR within the semiclassical Boltzmann framework.[56–58] However, these descriptions are under certain conditions and it seems that Dieny's phenomenological scattering and shunting analysis[55,59] is quite reasonable[4,58] and contains a significant part of the physics of the spin valve effect. In this analysis exponential and linear thickness dependences of GMR represent the scattering and shunting effects, respectively. The solid lines in Fig. 2 are fits based on Dieny's analysis.[55,59] These fits are for qualitative descriptions of our numerical data and are presented in order as follows: (a) $A\exp(-x/B)/(1+Cx)$, (b) $\{A[1-\exp(-x/B)]+D\}/(1+Cx)$, (c) and (d) $A[1-\exp(-x/B)]/(1+Cx)$, (e) $1/(1+Cx)$, and (f) $1/(1+Cx)$ and $A\exp(-x/B)+D/(1+Cx)$ for the NOL and non-NOL cases, respectively. The functions in (a)–(e) are applicable to both the NOL and non-NOL cases. In (b), an extra term D in the numerator seems to give a better fit, which emphasizes the shunting effect of the filter layer. The linear behaviors in (e) and (f) were fitted by $1/(1+Cx)$ with small C's. Note that B in these fits is not necessarily equivalent to the mean free path. It may correspond to the angular average of the mean free path[55] and its value may be smaller than that of the mean free path.[59,60]

The behaviors observed in Figs. 2(e) and 2(f) are worthy of more discussion. Regarding the critical part CoFe/Cu/CoFe of the BSV as shown in Fig. 1, the influence of the left Ta layer (Ta^l) on the GMR should be less than that of the right Ta layer (Ta^r). One reason is that on the left side, the IrMn layer has a small MFP and thus will block the carriers in Ta^l to transport to the critical region, while on the right side the Cu filter, with large MFP, will permit carriers in Ta^r to transport to the critical region quite easily. Another reason is that Ta^l is farther from the critical region than Ta^r. Due to these two reasons, the transport in Ta^l cannot have a critical influence on the GMR of the entire SV structure and thus, only the shunting effect, which is characterized by a linear behavior, is demonstrated for d_{Ta^l}. On the other hand, a different behavior is exhibited for d_{Ta^r}: there is an initial fast drop of GMR with increasing d_{Ta^r}. Regarding this drop, we have found through our simulations the following.

(i) At small d_{Ta^r}, the sheet resistance decreases with decreasing d_{Ta^r}. It has been found that when d_{Ta^r} is very thin, the sheet resistance (both parallel and antiparallel) is very small because the bulk of the carriers that arrive at the outer surface of Ta^r will be specularly reflected. The sheet resistance begins to increase with increasing d_{Ta^r} because the bulk scattering of the short MFP Ta layer begins to come into effect and eventually fewer carriers are transported back into the critical region. Finally, when d_{Ta^r} is too thick, the surface specular reflection loses its function but the shunting effect becomes dominant, and again the sheet resistance becomes small.

(ii) The change in sheet resistance increases with decreasing d_{Ta^r}.

(i) and (ii) together explain the initial drastic decrease of GMR with increasing d_{Ta^r}, as observed in the bottom curve in Fig. 2(f).

Like a layer with small MFP, say IrMn, a NOL with large specular reflection will efficiently block the transport of carriers normal to the layer. In this sense, the addition of the NOL at position 15 after the Cu filter layer will render the prototype BSV structure (with IrMn at the bottom) more "symmetric." Such an added NOL is very far from Ta^l and will have little influence on the carriers within Ta^l. Hence, the shunting effect of Ta^l will remain [see the upper linear behavior in Fig. 2(e)]. However, the added NOL is just adjacent to Ta^r and will efficiently block the carriers in Ta^r. Hence, the fast-drop behavior is washed out by the NOL and the shunting effect manifests itself as the linear curve at the upper part of Fig. 2(f).

Interestingly, the fast-drop behavior in Fig. 2(f) can still remain if the NOL is inserted at IrMn/CoFe (or inside the pinned layer) instead of Cu/Ta. The reason is that such a NOL is quite far from Ta^r and thus cannot smear the fast-drop behavior.

The MFP plays an important role in shaping the trend of GMR against thickness of a certain layer. The length scale spanned by the fast drop is primarily related to the MFP of Ta: by keeping λ_{Ta^l} short as 6 Å while assuming $\lambda_{\mathrm{Ta}^r}=60$ Å, it was found that GMR gradually decreases with increasing d_{Ta^r}, in the form of $A\exp(-x/B)+D$, where B is about 43 Å.

Similarly, Dieny[53] found that in trilayers the majority MFP plays an important role for the GMR variation with the thickness of the ferromagnetic layer while in multilayers it is the minority MFP responsible for the corresponding shape. As is well known, a SV is basically a trilayer structure; if a NOL with high specular reflection is added, the SV may function as a multilayer structure due to "the superlattice effect."[29] Hence, it is natural that the bottom and top curves

in Fig. 2(c) are closely related to the majority and minority MFP's of the free layer, respectively.

NOL specular reflection may effectively increase the number of carriers (both majority and minority) in the critical region of the SV. The increase of the density of minority carriers will make the minority carriers experience the ferromagnetic layer, causing the minority MFP of the ferromagnetic layer to play a role in determining the GMR variation with the thickness of the ferromagnetic layer, see the top curve in Fig. 2(c). On the other hand, in the case without NOL, more electrons will be transported to or scattered in the non-critical region of the SV and the reduction of the number of minority carriers causes the majority carriers to play the dominant role in determining the trend of GMR against the ferromagnetic layer, as we can see in the two bottom curves in Figs. 2(c) and 2(d).

We have seen in Fig. 2(c) that the NOL curve (top) is different from the non-NOL plot (bottom); however, the trends with and without NOL in Fig. 2(d) are similar to each other and are thus both determined by the majority MFP of the pinned layer. The underlying reason is the distance effect. The position of the NOL inserted at the Cu/Ta (filter layer/capping layer) interface is nearer to the free layer than to the pinned layer (due to the Cu spacer). Due to large specular reflection of the nearby NOL, a large number of minority carriers can sample the free layer and their effect to GMR is manifest as the top curve in Fig. 2(c). However, due to the long distance from the NOL at Cu/Ta to the pinned layer and due to the short minority mean free paths of the free and pinned layers, the number of the specular-reflected minority carriers in the pinned layer should be less than that of the free layer and hence it is only the majority carriers that play the role in determining the trend of GMR against the thickness of the pinned layer, see the top curve in Fig. 2(d).

When we turn to the NOL insertion at the IrMn/CoFe interface, interesting results are observed: the top curve in Fig. 2(d) will bear the feature of the top curve in Fig. 2(c) and vice versa. It is clear that such a NOL insertion enables the minority (majority) carriers to sample the pinned (free) layer since the NOL is now adjacent to the CoFe pinned layer but farther from the CoFe free layer (distance effect). Note that the switching of the curves was also numerically obtained in the case of the NOL insertion inside the pinned layer, an issue that may be experimentally examined.

Before ending this subsection, it is worth mentioning that (i) approximate linear dependences of GMR have been obtained for the thickness of the under layer NiFe and the AFM layer IrMn, in both NOL and non-NOL cases. (ii) As for the variations of the GMR ratio with the thickness of the NOL itself, linear behavior is obtained for all of the positions except those before, inside, and after the Cu spacer where exponential decays were found.

B. Optimization of NOL insertion positions

Now we shall address the variation of GMR with the different NOL insertion positions as shown in Fig. 1. The results obtained are presented in Fig. 3. It seems that the effects of the NOL insertion positions can be divided into three

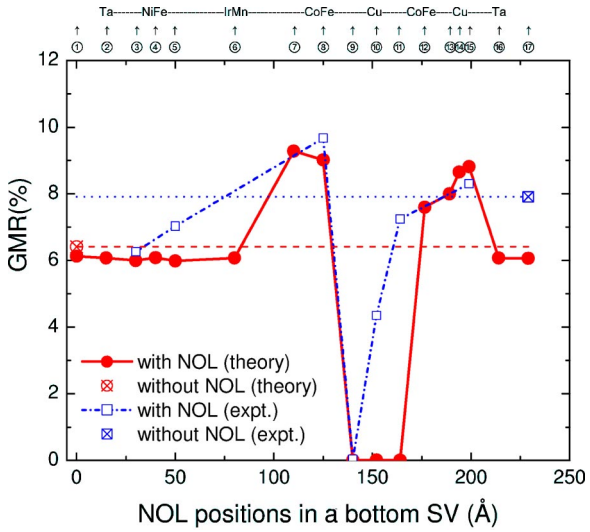

FIG. 3. (Color online) Calculated (circles) GMR ratios at different NOL positions in a bottom spin valve, compared with our experiments (squares). The dashed (dotted) line, representing the calculated (measured) GMR value without NOL, is a guide to the eye.

groups. (i) Inactive positions 1–6, 16, and 17 where GMR is slightly reduced. These positions are outside the pinned and filter layers. (ii) Ferromagnetic and filter positions 7, 8, and 12–15 where GMR is enhanced. (iii) Spacer positions 9, 10, and 11 where GMR is dramatically suppressed. Position 9 (11) is the pinned layer/spacer (spacer/free layer) interface while position 10 is at the center of the spacer.

The reduction of GMR at the inactive positions can be understood by the thickness effect of the inserted oxide layer. The addition of the oxide layer into these relatively inactive layers only makes the SV thicker and thus results in a stronger shunting effect, so the GMR ratio decreases.

The GMR enhancements by the NOL insertions inside the pinned layer (position 8) and after the CoFe free layer (position 13) are consistent with the corresponding pioneering experiments (see Refs. 10 and 22, respectively) and a recent work.[38] The enhancements at position 8 inside the pinned layer and at position 15 after the Cu filter layer are consistent with our experiments, see Fig. 3. Like the cases in Fig. 2, the GMR enhancements observed here should be ascribed to the NOL specular reflection. Such reflection would increase the number of electrons transported in the critical region of the SV. At the same time, this reflection maintains the spin directions. Hence, the spin-dependent transport is amplified, leading to the GMR enhancements.

However, the specular reflection may destroy GMR when the oxide layer is placed before, inside, and after the Cu spacer, as shown in Fig. 3 for positions 9, 10, and 11, respectively. A highly reflecting specular layer positioned in these places would prevent electrons from transporting from one ferromagnetic layer to another ferromagnetic layer via the Cu spacer, which may be termed as the blocking effect: if electrons are from the pinned layer, they will be reflected back and will not sense whether the direction of the free layer is changed or not. Therefore, there is no GMR effect; if electrons are from the ferromagnetic free layer, there are either

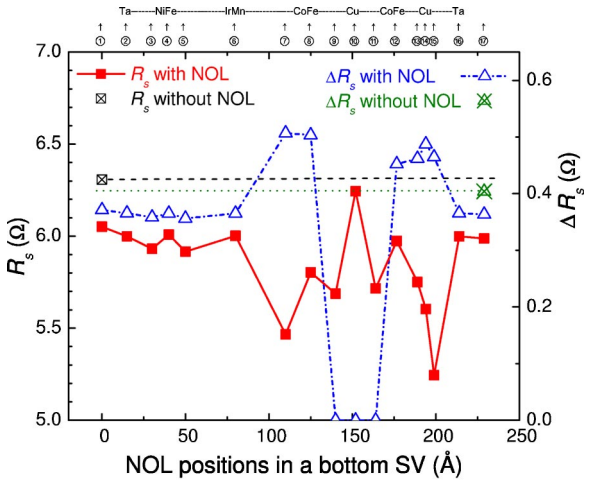

FIG. 4. (Color online) Sheet resistance R_s (squares) and change in sheet resistance ΔR_s (triangles) of different NOL insertion positions. The dashed line represents the R_s value without NOL.

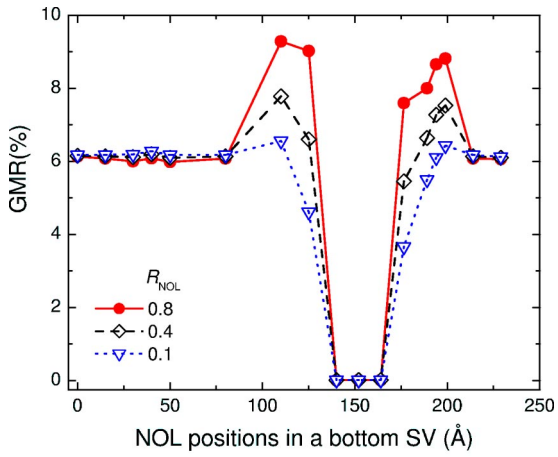

FIG. 5. (Color online) GMR vs NOL positions for spin-independent NOL specular reflections.

spin-up or spin-down majority carriers depending on the direction of the magnetization of the free layer since the minority carriers may be ignored due to their short MFP. Upon specular reflection (blocking), the spin direction of each kind of majority carriers remains unchanged. If the specular reflection is spin independent, then there should be no difference between the two sorts of polarized currents consisting of the two kinds of majorities. Thus, no GMR or only a small GMR effect can be obtained.

The theoretically obtained very small GMR at position 9 between the pinned CoFe layer and the Cu spacer is consistent with our experimental result (see Fig. 3). Such a dramatic suppression was also experimentally observed by Lai *et al.*[61] However, the GMR ratios measured at positions 10 and 11 are relatively large (see Fig. 3) and this might be due to the mobility of oxygen:[22] oxygen may diffuse into the CoFe free layer and thus the Cu/CoFe junction may have a non-sharp interface. Similarly, intermixing between Cu and CoFe may also contribute to the formation of the non-sharp interface of Cu/CoFe.[23]

Since the number of electrons is effectively increased due to the NOL specular reflection, the conductance should be increased. The corresponding decrease in the sheet resistance R_s (hereafter $R_s^{\uparrow\uparrow}$ is referred to as R_s) is presented in Fig. 4 (see squares), together with the difference between the antiparallel and parallel resistances, ΔR_s (see triangles). It can be seen that R_s in all the insertion locations are lowered, compared to the R_s without NOL. The pattern of ΔR_s against the NOL insertion positions is similar to that of GMR (cf. Fig. 3). Such similarity was also observed in the case of O_2 exposure in our experiments.[15]

Table I is a summary of our experimental optimizations, together with the corresponding theoretical results. The comparison between the theory and experiment shows overall good agreement. Upon the NOL insertion after the AFM layer (position 7), our theory predicts that the GMR ratio is enhanced while the actual experimental finding is relatively small. This contradiction is likely due to the deleterious effect of the NOL on the pinning field of the antiferromagnetic layer.

In Fig. 5, GMR ratios against the NOL insertions for different values of the spin-independent NOL specular reflection are presented. It can be seen that with increasing NOL specular reflection, the GMR ratios of the NOL insertion at the ferromagnetic and filter positions are enhanced. How-

TABLE I. Theoretical and experimental summaries of NOL-affected GMR, sheet resistance, and change in sheet resistance. ↑ (↓) means the value increased (decreased), compared to the corresponding value without NOL.

	GMR		R_s		ΔR_s	
NOL position	Calc.	Expt.	Calc.	Expt.	Calc.	Expt.
After seed layer (3)	↓	↓	↓	↓	↓	↓
After under layer (5)	↓	↓	↓	↓	↓	↓
After AFM layer (7)	↑	⇓	↓	↓	↑	⇓
Inside pinned layer (8)	↑	↑	↓	↓	↑	↑
Before spacer layer (9)	↓	↓	↓	↓	↓	↓
Inside spacer layer (10)	↓	↓	↓	↓	↓	↓
After spacer layer (11)	↓	↓	↓	↓	↓	↓
After free layer (13)	↑	↑	↓	↓	↑	↑
After filter layer (15)	↑	↑	↓	↓	↑	↑

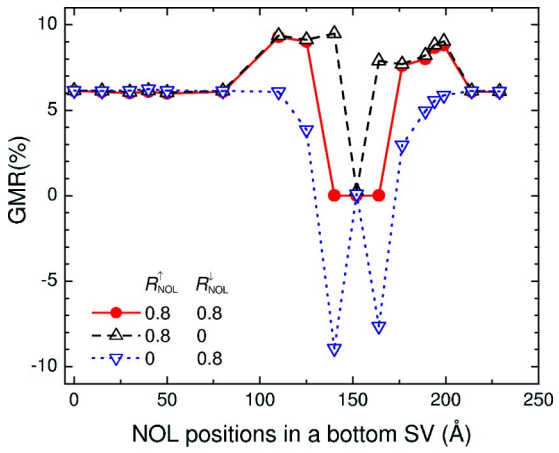

FIG. 6. (Color online) GMR vs NOL positions for spin-dependent NOL specular reflections.

ever, when the NOL specular reflection is small, the GMR is not so large at the ferromagnetic positions, which may be due to the trade-off between specular reflection and shunting. Note that varying the NOL specular reflection has little influence on the GMR ratios upon the NOL insertions in the spacer and in the inactive layers.

Optimization of the NOL positions has also been performed for spin-dependent NOL specular reflection as shown in Fig. 6. It can be seen that the GMR is enhanced at the ferromagnetic and filter positions by the majority reflection ($R^{\uparrow}_{\mathrm{NOL}}=0.8$, $R^{\downarrow}_{\mathrm{NOL}}=0$) while it is reduced in the case of the minority reflection ($R^{\uparrow}_{\mathrm{NOL}}=0$, $R^{\downarrow}_{\mathrm{NOL}}=0.8$). The enhancement of GMR due to the majority reflection mainly follows the pattern of GMR due to the spin-independent specular reflection ($R^{\uparrow}_{\mathrm{NOL}}=R^{\downarrow}_{\mathrm{NOL}}=0.8$). Hence, one may infer that the majority carriers play a decisive role in determining GMR.

In the suppressed spacer area, spin-dependent NOL specular reflection results in an interesting finding, i.e., the inverse GMR[62] (see Fig. 6). The GMR ratios are very high at positions 9 and 11 for the majority reflection. On the other hand, the GMR ratio is still high but now negative at positions 9 and 11 for the minority reflection. In the case of both majority and minority reflections ($R^{\uparrow}_{\mathrm{NOL}}=R^{\downarrow}_{\mathrm{NOL}}=0.8$), the GMR ratios at positions 9 and 11 are nearly zero. These results seem to suggest that the GMR phenomenon at these two positions is an average effect of different spins. In fact, in virtue of the contributions of different spin channels (i.e., Mott's two fluid model[63]) to the sheet conductance [σ_s, which is the reciprocal of the sheet resistance R_s in Eq. (10)], the GMR ratio may be written as

$$\begin{aligned}\mathrm{GMR}&=\frac{\sigma_s^{\uparrow\uparrow}-\sigma_s^{\uparrow\downarrow}}{\sigma_s^{\uparrow\downarrow}}\\&=\frac{[(\sigma_s^{\uparrow\uparrow})^{\uparrow^e}-(\sigma_s^{\uparrow\downarrow})^{\uparrow^e}]+[(\sigma_s^{\uparrow\uparrow})^{\downarrow^e}-(\sigma_s^{\uparrow\downarrow})^{\downarrow^e}]}{\sigma_s^{\uparrow\downarrow}}\\&=\frac{(\Delta\sigma_s)^{\uparrow^e}+(\Delta\sigma_s)^{\downarrow^e}}{\sigma_s^{\uparrow\downarrow}}.\end{aligned}\tag{13}$$

It is clear that for the study of our prototype BSV, $(\sigma_s^{\uparrow\uparrow})^{\uparrow^e}>(\sigma_s^{\uparrow\downarrow})^{\uparrow^e}$ and $(\sigma_s^{\uparrow\uparrow})^{\downarrow^e}<(\sigma_s^{\uparrow\downarrow})^{\downarrow^e}$. Hence, $(\Delta\sigma_s)^{\uparrow^e}>0$ and $(\Delta\sigma_s)^{\downarrow^e}<0$, respectively. These different channels with opposite signs are apparent upon the NOL insertions inside the interfaces of spacer and ferromagnetic layers, i.e., at positions 9 and 11 as shown in Fig. 6. Clearly, the average effect of the two different spin channels may also explain the suppressed GMR in Fig. 3, where the interpretation was given in terms of the blocking effect. Note that the small GMR ratios at position 10 in Fig. 6 are due to the effective blocking of spin quantization since in this case, the spin quantization x axis is placed in the middle of the NOL instead of the spacer (cf. Fig. 1). By placing the quantization axis outside the NOL layer and inside the spacer, inverse GMR and the average effect were also found for position 10.

Figures 3 and 5 have shown that to achieve large GMR in SV's, electrons should be able to transmit between the two ferromagnetic layers, as pointed out in Refs. 58 and 59. However, Fig. 6 implies that there is no need for electrons to transport between the two ferromagnetic layers [note that even by setting $T_{\mathrm{NOL}}=0$, large positive and inverse GMR ratios can still be obtained for $R^{\uparrow}_{\mathrm{NOL}}=0.8$ ($R^{\downarrow}_{\mathrm{NOL}}=0$) and $R^{\downarrow}_{\mathrm{NOL}}=0.8$ ($R^{\uparrow}_{\mathrm{NOL}}=0$), respectively]. Hence, we here predict a GMR device composed of a free layer and a spin-dependent specular reflection layer. The spin-dependent specular reflection may be attainable by a hard layer with large coercivities[28] or by some half metals (see Ref. 64 and references therein). Note that a spacer layer is perhaps necessary to reduce the coupling imposed on the free layer.

C. Specularity

As seen in the previous subsections and as generally believed, an important characteristic of specular reflection is to enhance GMR. However, this feature deserves more discussion. In Fig. 7, we have plotted GMR ratios as a function of specular reflections in the following situations.

(a) NOL specular reflection: NOL inside the pinned layer, at the Cu/Ta interface and outside the capping layer with different MFP's.

(b) Interface specular reflection: interface of IrMn/CoFe (with and without NOL at Cu/Ta) and interface of Cu/Ta (with and without NOL in the pinned layer).

(c) Surface specular reflection ($p_{l\sigma}=p_{r\sigma}=p$): the left and right Ta surface layers are of different mean free path, with and without NOL inside the pinned layer.

(d) Specularity factor: it is spin independent ($S_{\uparrow}=S_{\downarrow}=S$) or dependent ($S_{\uparrow}=S$, $S_{\downarrow}=S/2$), with and without NOL inside the pinned layer.

From Fig. 7, we can conclude the following.

(i) The GMR ratio increases with increasing specularity, as usually expected. An exception is that upon increasing specularity a very slight reduction of GMR occurs in the cases of Ta with short mean free path (6 Å), see the dotted line in Fig. 7(a) and the full and dashed lines in Fig. 7(c); see also the corresponding enlarged plots in Fig. 8. A simple explanation to the exception will be given in the discussion of Fig. 9.

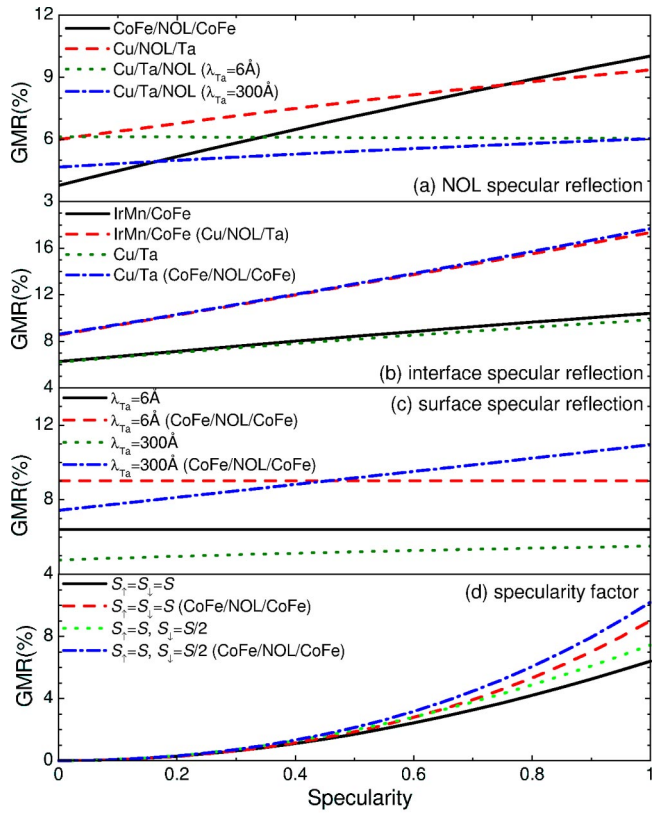

FIG. 7. (Color online) GMR ratios as a function of (a) NOL specular reflection R_{NOL}, (b) interface specular reflection R, (c) surface specular reflection p, and (d) specularity factor S. In the figure, CoFe refers to the pinned layer.

(ii) The specularity dependences of GMR are further enhanced upon appropriate NOL insertions [see Figs. 7(b)–7(d)].

(iii) The specularity dependence of GMR is also enhanced by spin asymmetry [$S_{\uparrow}=S$, $S_{\downarrow}=S/2$, see the dotted and chain-dotted lines in Fig. 7(d)].

Figure 9 shows GMR, R_s, and ΔR_s as a function of the NOL insertion positions for different surface reflections and mean free paths of Ta. First of all, it should be emphasized that to focus on the surface reflections here, the NOL is now assumed very thin ($d_{\mathrm{NOL}}=1$ Å) and highly transmitting ($T_{\mathrm{NOL}}=1$, $R_{\mathrm{NOL}}=0$, and $\lambda_{\mathrm{NOL}}^{\uparrow\downarrow}=300$ Å). Such a NOL inserted at any position will allow electrons to transport freely through the SV and clearly, there will be no optimized NOL insertion positions. In this case, the obtained values of GMR, R_s, and ΔR_s are close to the respective values without NOL. Second, overall reductions of GMR, R_s, and ΔR_s are observed when λ_{Ta} changes from 6 Å to 300 Å, see data of triangles compared to those of squares and circles in Fig. 9. Finally, the surface specular reflections of p_l and p_r play an unimportant (important) role on GMR, R_s, and ΔR_s at short (long) λ_{Ta}. When the values of p_l and p_r change from 0 to 1, for short λ_{Ta} there are very slight reductions for all of the quantities of GMR, R_s and ΔR_s (circles compared to squares); for long λ_{Ta} there are considerable reductions for only R_s and ΔR_s [up triangles compared to down triangles in Figs. 9(b) and 9(c)] and a notable enhancement for GMR [up triangles compared to down triangles in Fig. 9(a)]. This enhancement of GMR at long λ_{Ta} is as expected, contrary to the slight reduction behavior at short λ_{Ta}. A simple explana-

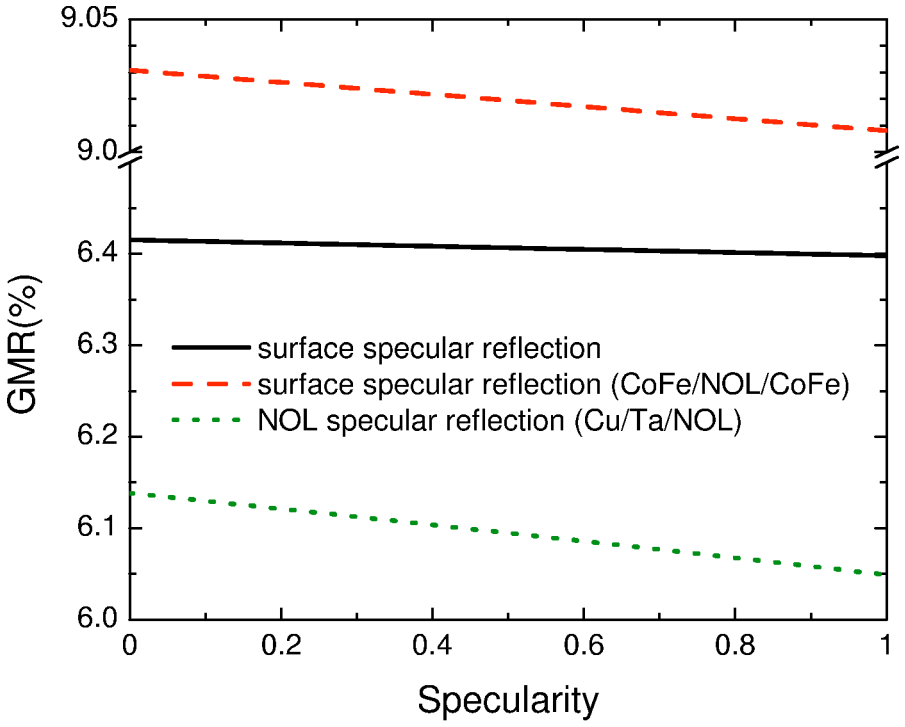

FIG. 8. (Color online) Enlarged view of the decreasing trends of GMR against specularity for surface specular reflection p (with and without NOL) and NOL specular reflection R_{NOL} (cf. Fig. 7). In the figure, CoFe refers to the pinned layer.

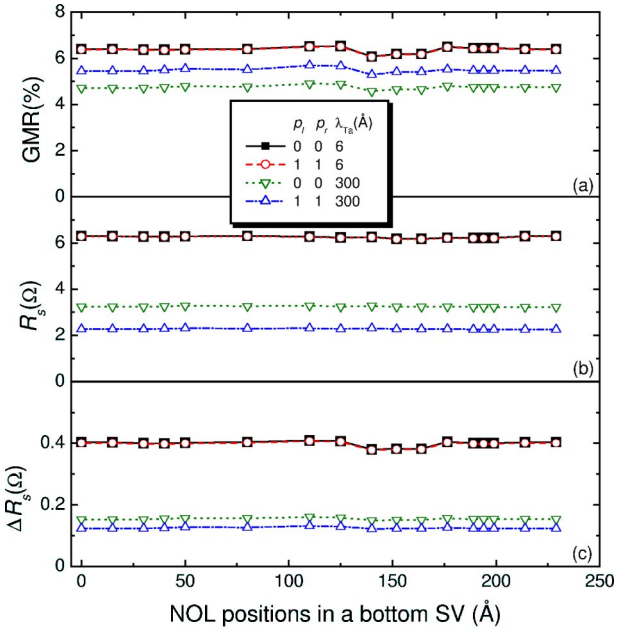

FIG. 9. (Color online) GMR ratios, sheet resistance, and change in sheet resistance as a function of NOL insertion positions for different surface reflectivities and different mean free paths of Ta. Here, the inserted NOL is assumed very thin and highly transmitting, thus showing little NOL insertion effects.

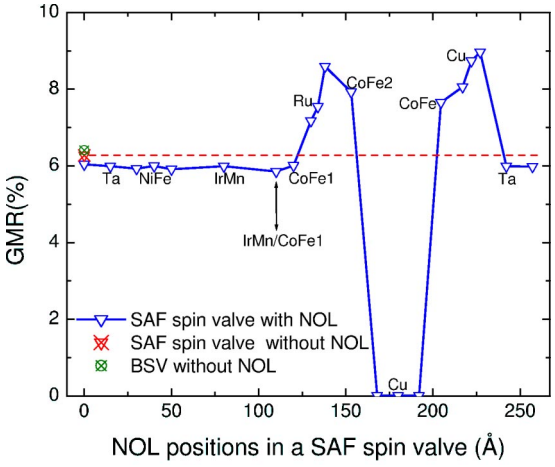

FIG. 10. (Color online) GMR ratios at different NOL insertion positions in a synthetic antiferromagnetic (SAF) spin valve with the structure of Ta/NiFe/IrMn/CoFe1/Ru/CoFe2/Cu/CoFe/Cu/Ta.

tion to these usual and unusual behaviors may be rationalized in the following way. When surface specular reflection increases, the reduction of sheet resistance can be expected (cf. Fig. 4). In fact, according to Ref. 65, the sheet resistance of a specified layer can be written as

$$R_s^{i\sigma}=\rho_{i\sigma}\left[\frac{1}{\lambda_{i\sigma}}+\frac{3}{8d_i}\left(1-\frac{p_{i\sigma}+q_{i\sigma}}{2}\right)\right],\quad (d_i\gg\lambda_{i\sigma}),\quad (14)$$

$$R_s^{i\sigma}=\rho_{i\sigma}\frac{4}{3}\frac{1-p_{i\sigma}q_{i\sigma}}{(1+p_{i\sigma})(1+q_{i\sigma})}\frac{1}{d_i\ln(\lambda_{i\sigma}/d_i)},\quad (d_i\ll\lambda_{i\sigma}),\quad (15)$$

where $\rho_{i\sigma}=m_{i\sigma}v_{Fi\sigma}/e^2n_{i\sigma}d_i$ with $n_{i\sigma}$ being the electron density. $p_{i\sigma}$ and $q_{i\sigma}$ are the specular factors of the two surfaces of the layer. Both equations show that the sheet resistances of the layer decrease with increasing specular factors and mean free paths. The corresponding increase of the sheet conductances of the layer will result in the reduction of the sheet resistance R_s of the entire SV structure. As for ΔR_s, it may be either increased or decreased. If it is increased or its decreasing speed is slower than the decreasing speed of R_s, the resulting GMR will be enhanced. If the decreasing speed of ΔR_s is so fast that it cannot compensate the drop in R_s, then the GMR ratio will be reduced. This explanation is also applicable to the exception observed in Fig. 7.

Recently, Tsymbal and Pettifor[4] and Butler *et al.*[35] have also pointed out that surface specular reflection may reduce GMR if the ferromagnetic layer is too thick[4] or the majority mean free path in the ferromagnetic layer is sufficiently short.[35] Here, it might be intuitively natural that carriers transporting in a capping layer with a short MFP and a high surface specular reflection will be effectively localized or confined within the layer. The reason is that the short MFP and the high surface specular reflection may form a reflection-induced channel since the short MFP may be equivalent to specular reflection to a certain extent. This channeling or localized effect may not only explain the exceptions observed in Figs. 7–9 but also possibly explain the slight reduction of GMR when the NOL is inserted in the inactive regions where the layers of SV's, say Ta and IrMn, are mainly characterized by short MFP's (see Fig. 3). Moreover, this effect implies that certain *rough* interfaces of SV's may result in *large* GMR, as confirmed by our numerical simulations: GMR increases with decreasing specular reflection of the interfaces at Ta/NiFe, NiFe/IrMn, pinned layer/spacer, and spacer/free layer of our prototype BSV.[49] However, these results should be treated with caution. For example, a good antiferromagnetic configuration between the free and pinned layers would prefer smooth interfaces at pinned layer/spacer and spacer/free layer. It should be mentioned that the channeling or localized effect described here is different from those in Refs. 29, 33, and 66 although it seems that ''reflection'' plays a common role in all of these channeling effects.

Egelhoff *et al.*[16] have conducted interesting experiments on specular effects of Ta. Based on the fact that Ta suppresses the specular scattering, they concluded that Ta is a bad choice for a protective coating on a spin valve. Their conclusion is at least true in the sense that Ta suppresses the interface specular reflection at Cu/Ta, which is detrimental to GMR [see the dotted line in Fig. 7(b)]. However, the suppression of the surface specular reflection is beneficial to GMR [see the full line in Fig. 7(c)]. Moreover, the blocking property of the top Ta layer (with short MFP) for a BSV is equivalent to the blocking effect of high specular reflection to a certain degree. Hence, one may expect that a top layer with short MFP is still a possible choice for protecting spin

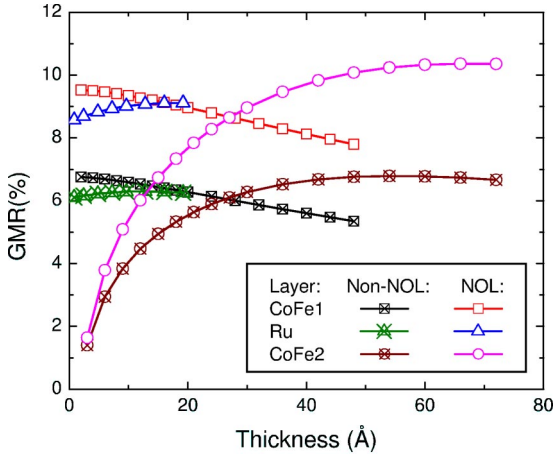

FIG. 11. (Color online) GMR ratios as a function of thickness of each layer of the SAF structure, CoFe1/Ru/CoFe2. Symbols without × indicate the cases of the NOL insertion at the Cu/Ta interface.

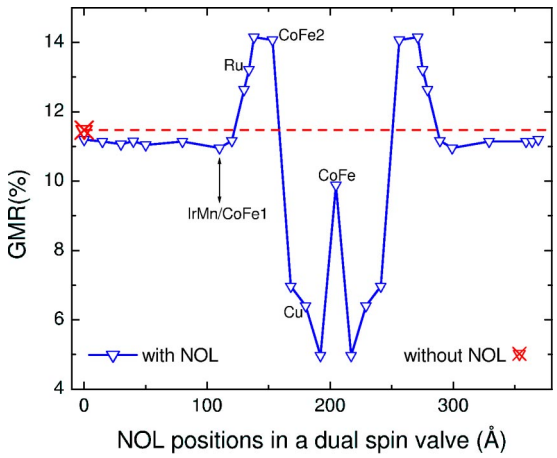

FIG. 12. (Color online) GMR ratios at different NOL insertion positions in a dual spin valve with the structure of Ta/NiFe/IrMn/CoFe1/Ru/CoFe2/Cu/CoFe/Cu/CoFe2/Ru/CoFe1/IrMn/Ta.

valves. Similarly, one may explain the high GMR ratio of spin valves with a top layer of NiO (Ref. 19) that has a small surface specularity.[67]

D. Synthetic antiferromagnetic spin valves

The theory in Sec. III was also applied to synthetic antiferromagnetic (SAF) spin valves,[68] which are of current interest to the HDD industry.[69,70] The SAF spin valve studied here consists of Ta (30)/ NiFe (20)/ IrMn (60)/ CoFe1 (20)/ Ru (8)/ CoFe2 (30)/ Cu (24)/ CoFe (25)/ Cu (10)/ Ta (30) (thickness in Å, cf. Fig. 10). The SAF layers CoFe1/Ru/CoFe2 replace the pinned layer CoFe in the prototype BSV. For the Ru layer, we choose: $d_{\mathrm{Ru}}=8$ Å and $\lambda_{\mathrm{Ru}}^{\uparrow\downarrow}=30$ Å.[32] For comparison, the values of all other parameters are set the same as those of the prototype BSV. Note that $\lambda_{\mathrm{CoFe1}}^{\uparrow}<\lambda_{\mathrm{CoFe1}}^{\downarrow}$ and $\lambda_{\mathrm{CoFe2}}^{\uparrow}>\lambda_{\mathrm{CoFe2}}^{\downarrow}$ have been assumed to simulate the antiferromagnetic coupling between CoFe1 and CoFe2 at $d_{\mathrm{Ru}}=8$ Å.

The variation of GMR with the NOL insertion locations is presented in Fig. 10. The general pattern is quite similar to the counterpart in Fig. 3. However, upon the NOL insertion at the IrMn/CoFe1 interface (see the location indicated by the arrow in Fig. 10), the GMR ratio is smaller than that without NOL (down-triangle with ×) and this property is opposite to the BSV case, where the GMR ratio with the NOL inserted at IrMn/CoFe (position 7 in Fig. 3) is larger than that without NOL (circle with × in Fig. 3). Note that this difference was obtained under $\lambda_{\mathrm{CoFe1}}^{\uparrow}<\lambda_{\mathrm{CoFe1}}^{\downarrow}$. If we choose $\lambda_{\mathrm{CoFe1}}^{\uparrow}>\lambda_{\mathrm{CoFe1}}^{\downarrow}$, the difference then disappears. Note also that inverse GMR, whose pattern was nearly the vertical flip of that in Fig. 10, can be achieved if we choose $\lambda_{\mathrm{CoFe2}}^{\uparrow}<\lambda_{\mathrm{CoFe2}}^{\downarrow}$ whether $\lambda_{\mathrm{CoFe1}}^{\uparrow}>\lambda_{\mathrm{CoFe1}}^{\downarrow}$ or $\lambda_{\mathrm{CoFe1}}^{\uparrow}<\lambda_{\mathrm{CoFe1}}^{\downarrow}$.

It should be pointed that the GMR ratio in the SAF spin valve without NOL (down triangle with ×) is smaller than the counterpart in the BSV (circle with ×), see Fig. 10. This conclusion was drawn at $d_{\mathrm{CoFe2}}=30$ Å. Even by setting the SAF structure as CoFe1 (10)/ Ru (8)/ CoFe2 (20), where $d_{\mathrm{CoFe1}}+d_{\mathrm{CoFe2}}=d_{\mathrm{CoFe}}$ (pinned layer in the BSV), the same conclusion also holds and this is consistent with the theoretical and experimental work of Ref. 71.

It was found that almost all the results presented in Figs. 2–9 can be reproduced in our SAF simulations provided that the role of the pinned CoFe layer of the BSV was occupied by CoFe2 of the SAF spin valve and IrMn/CoFe in Fig. 7(b) was replaced by Ru/CoFe2. In Fig. 11, we focus on the thickness dependences of GMR for the SAF structure of CoFe1/Ru/CoFe2, with and without the NOL inserted at Cu/Ta. It can be seen that the GMR variations with d_{CoFe1} are linear and the GMR trends against d_{CoFe2} are quite similar to those in Fig. 2(d). Hence, CoFe1 acts as a shunting layer and CoFe2 plays the role of the pinned layer for the SAF spin valve. The GMR variations with the thickness of CoFe1 and CoFe2 obtained here are in reasonable agreement with the quantum mechanical treatments except oscillations.[71] Note that the trend of GMR against the Ru thickness (without NOL) in Fig. 11 is in good qualitative agreement with the experimental work of Ref. 72.

E. Dual spin valves

The semiclassical theory[24,25] in Sec. III has been extended to study dual spin valves.[73] To our knowledge, this is done for the first time. To do so, the spin quantizations occurring in the two spacers of the dual spin valve have to be taken into account simultaneously and thus, two additional equations, equivalent to Eqs. (3d) and (3e), are required. The dual spin valve studied here consists of Ta (30)/ NiFe (20)/ IrMn (60)/ CoFe1 (20)/ Ru (8)/ CoFe2 (30)/ Cu (24)/ CoFe (25)/ Cu (24)/ CoFe2 (30)/ Ru (8)/ CoFe1 (20)/ IrMn (60)/Ta (10) (thickness in Å, cf. Fig. 12). For consistency, the values of all the parameters are set the same as those of the prototype BSV and the SAF spin valve.

Shown in Fig. 12 are the impressive overall large GMR ratios, compared to the corresponding cases in the single and the synthetic SV's in Figs. 3 and 10, respectively. The large GMR here is merely attributed to doubling the number of

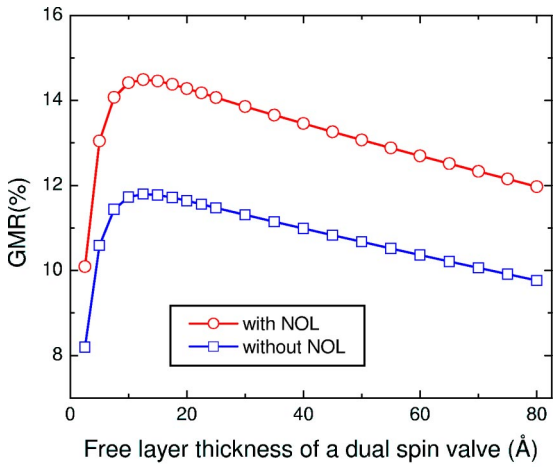

FIG. 13. (Color online) GMR ratios as a function of thickness of the free layer of a dual spin valve. The NOL is inserted inside CoFe2 located either on the left or right side of the dual spin valve.

spin-dependent bulk scattering events since the interface parameters of S, T, and R in our simulations have been assumed spin independent and the surface specular conditions have minor influences on GMR [see the full line in Fig. 7(c)]. This attribution is different from that in Ref. 74 where the roles of surfaces and interfaces were emphasized. A striking feature is also noteworthy in Fig. 12: the GMR is suppressed by the NOL insertion inside the free layer. This feature is probably due to the NOL blocking: it was found that compared to the non-insertion case, the GMR was enhanced by inserting a very thin and highly transmitting NOL inside the free layer.

It was found that most results obtained for the dual spin valve are quite similar to those of the single and the synthetic spin valves presented in the previous subsections. However, there is one prominent exception: in the non-NOL case, the trend of GMR against the thickness of the free layer is similar to that in a multilayer[52,53] and thus similar to the corresponding NOL case (see Fig. 13). The similarity between the NOL and non-NOL cases is quite different from the counterparts in Fig. 2(c). This difference is caused by the short minority MFP of the free layer coming into effect in dual spin valves. By lengthening the short MFP, we found that the difference disappears and a gradual increase with the thickness of the free layer can be obtained. This increasing trend is qualitatively consistent with the experiment of Egelhoff *et al.*, see the bottom curve of Fig. 2 in Ref. 75. Note that the top curves of Fig. 2 in the same reference demonstrated the case of the composite free layer Co/NiFe/Co where the trend of GMR against the thickness of NiFe is decreasing. This decreasing trend can be understood as shunting and in this case, the corresponding thickness can be considerably reduced (see also Fig. 13).

V. SUMMARY

A semiclassical theory has been developed, verified, and applied to the NOL effects in single, synthetic, and dual spin valves. Most results obtained for the single spin valves are directly applicable to synthetic and dual spin valves with appropriate modifications.

Theoretical optimization of the NOL insertion positions for a realistic bottom spin filter spin valve, together with the study of the sheet resistances, is in good overall agreement with experiments. Generally speaking, GMR is a strong function of the specular reflection of the NOL inserted in the pinned, free, and filter layers while it is relatively weakly dependent on the specular reflection of the NOL inserted inside the spacer and in the inactive layers outside the pinned and filter layers. More specifically, we have the following.

(i) GMR enhancements are confirmed for the insertion inside the pinned layer and after the free and filter layers. The enhancements are more prominent with larger specular reflections and most probably due to the contribution of the majority carriers.

(ii) Due to the blocking effect, highly reflecting NOL placed before, inside, and after the Cu spacer usually leads to a dramatic suppression of GMR. The average effect of different spin channels may also explain this dramatic suppression. By considering spin-dependent NOL specular reflections before or after the Cu spacer, large inverse and positive GMR effects were demonstrated. Hence, spin-dependent specular reflection opens up the possibility of a GMR device with simple structures.

(iii) Due to shunting (or possibly the channeling effect), GMR is reduced for the NOL insertion in the inactive layers such as the seed, under, and capping layers.

(iv) The channeling effect possibly explains the slight reduction of GMR in a realistic spin valve when the surface specular factor is changed from completely diffusive to purely specular. The direct cause for this slight reduction of GMR is the short mean free path of the capping layer, which prohibits the transport of the specularly reflected carriers into the critical region of spin valves.

Like a NOL, any layer with high interfacial specular reflection or with short bulk mean free path may have similar influences on the GMR. For example, a recent work[76] reveals that the Si layer inserted in the Cu spacer and the pinned layer results in suppression and enhancement of GMR, respectively. We have also shown that the properties of the interface and surface specular reflections are equivalent, to a certain degree, to those of the NOL insertions at the corresponding interfaces and surfaces (see Fig. 7). Thus, study of the NOL insertions and specular reflections helps understand properties of interfaces, surfaces, and layers (with blocking effect).

Dependences of GMR on various thicknesses of different layers of the single, synthetic, and dual spin valves are also studied for the NOL and non-NOL situations. The trends obtained (Figs. 2, 11, and 13) are consistent with existing literature and are in good agreement with Dieny's shunting and scattering analysis. The distance effect was also found: the distance from the inserted NOL to a certain layer may influence the shape of GMR against the thickness of that layer.

The GMR effect is multifaceted and it seems that one still cannot draw a universal conclusion regarding the oxide ef-

fects on spin valves (see Ref. 23 and references therein). The Boltzmann semiclassical theory, although highly phenomenological, has been very successful in explaining GMR, and we have demonstrated that it is adequate to the task of systematically analyzing the NOL insertion and specular effects in spin valves. This analysis may contribute to understanding the GMR mechanism and may serve as a useful guideline for practical optimization of the physical structure and the electrical properties of realistic spin valves.

ACKNOWLEDGMENTS

L.W. acknowledges discussions with G.C. Han, D. You, Z.B. Guo, and Y.K. Zheng; and help from H. Zhou.

*Electronic address: WANG_Li@dsi.a-star.edu.sg
†Electronic address: WU_Yihong@dsi.a-star.edu.sg

[1] M.N. Baibich, J.M. Broto, A. Fert, F. Nguyen Van Dau, F. Petroff, P. Eitenne, G. Creuzet, A. Friederich, and J. Chazelas, Phys. Rev. Lett. **61**, 2472 (1988).
[2] G. Binasch, P. Grünberg, F. Saurenbach, and W. Zinn, Phys. Rev. B **39**, 4828 (1989).
[3] P.P. Freitas, in *Spin Electronics*, edited by M. Ziese and M.J. Thornton (Springer-Verlag, Berlin, 2001), p. 464.
[4] E.Y. Tsymbal and D.G. Pettifor, in *Solid State Physics*, edited by H. Ehrenreich and F. Spaepen (Academic Press, New York, 2001), Vol. 56, p. 113.
[5] B. Dieny, V.S. Speriosu, S.S.P. Parkin, B.A. Gurney, D.R. Wilhoit, and D. Mauri, Phys. Rev. B **43**, 1297 (1991).
[6] B. Dieny, V.S. Speriosu, B.A. Gurney, S.S.P. Parkin, D.R. Wilhoit, K.P. Roche, S. Metin, D.T. Peterson, and S. Nadimi, J. Magn. Magn. Mater. **93**, 101 (1991).
[7] B. Dieny, V.S. Speriosu, S. Metin, S.S.P. Parkin, B.A. Gurney, P. Baumgart, and D.R. Wilhoit, J. Appl. Phys. **69**, 4774 (1991).
[8] B. Dieny, B.A. Gurney, S.E. Lambert, D. Mauri, S.S.P. Parkin, V. S. Speriosu, and D. R. Wilhoit, U. S. Patent No. 5,206,590 (April 27, 1993).
[9] C. Vouille, A. Barthélémy, F. Elokan, A. Fert, P.A. Schroeder, S.Y. Hsu, A. Reilly, and R. Loloee, Phys. Rev. B **60**, 6710 (1999).
[10] Y. Kamiguchi, H. Yuasa, H. Fukuzawa, K. Koui, H. Iwasaki, and M. Sahashi, *Digest of Intermag* (IEEE, New York, 1999), DB-01.
[11] A. Veloso, P.P. Freitas, P. Wei, N.P. Barradas, J.C. Soares, B. Almeida, and J.B. Sousa, Appl. Phys. Lett. **77**, 1020 (2000).
[12] M.F. Gillies and A.E.T. Kuiper, J. Appl. Phys. **88**, 5894 (2000).
[13] H. Sakakima, M. Satomi, Y. Sugita, and Y. Kawawake, J. Magn. Magn. Mater. **210**, L20 (2000).
[14] J. Hong, K. Noma, H. Kanai, and J. Kane, J. Appl. Phys. **89**, 6940 (2001).
[15] K.B. Li, Y.H. Wu, J.J. Qiu, G.C. Han, Z.B. Guo, H. Xie, and T.C. Chong, Appl. Phys. Lett. **79**, 3663 (2001).
[16] W.F. Egelhoff, Jr., P.J. Chen, C.J. Powell, M.D. Stiles, R.D. McMichael, J.H. Judy, K. Takano, A.E. Berkowitz, and J.M. Daughton, IEEE Trans. Magn. **33**, 3580 (1997).
[17] W.F. Egelhoff, Jr., P.J. Chen, C.J. Powell, D. Parks, G. Serpa, R.D. McMichael, D. Martien, and A.E. Berkowitz, J. Vac. Sci. Technol. B **17**, 1702 (1999).
[18] Y. Kawawake and H. Sakakima, IEEE Trans. Magn. **33**, 3538 (1997).
[19] H.J.M. Swagten, G.J. Strijkers, P.J.H. Bloemen, M.M.H. Willekens, and W.J.M. de Jonge, Phys. Rev. B **53**, 9108 (1996).
[20] W.F. Egelhoff, Jr., T. Ha, R.D.K. Misra, Y. Kadmon, J. Nir, C.J. Powell, M.D. Stiles, R.D. McMichael, C.-L. Lin, J.M. Sivertsen, J.H. Judy, K. Takano, A.E. Berkowitz, T.C. Anthony, and J.A. Brug, J. Appl. Phys. **78**, 273 (1995).
[21] H. Sakakima, Y. Sugita, M. Satomi, and Y. Kawawake, J. Magn. Magn. Mater. **198**, 9 (1999).
[22] W.F. Egelhoff, Jr., P.J. Chen, C.J. Powell, M.D. Stiles, R.D. McMichael, J.H. Judy, K. Takano, and A.E. Berkowitz, J. Appl. Phys. **82**, 6142 (1997).
[23] D.J. Larson, A.K. Petford-Long, A. Cerezo, S.P. Bozeman, A. Morrone, Y.Q. Ma, A. Georgalakis, and P.H. Clifton, Phys. Rev. B **67**, 144420 (2003).
[24] K. Fuchs, Proc. Cambridge Philos. Soc. **34**, 100 (1938).
[25] E.H. Sondheimer, Adv. Phys. **1**, 1 (1952).
[26] P.F. Carcia and A. Suna, J. Appl. Phys. **54**, 2000 (1983).
[27] R.E. Camley and J. Barnaś, Phys. Rev. Lett. **63**, 664 (1989).
[28] J. Barnaś, A. Fuss, R.E. Camley, P. Grünberg, and W. Zinn, Phys. Rev. B **42**, 8110 (1990).
[29] R.Q. Hood and L.M. Falicov, Phys. Rev. B **46**, 8287 (1992).
[30] H. Sakakima, E. Hirota, and Y. Kawawake, J. Magn. Magn. Mater. **184**, 49 (1998).
[31] K.B. Li, Y.H. Wu, and T.C. Chong, IEEE Trans. Magn. **36**, 2599 (2000).
[32] B. Dieny, M. Li, S.H. Liao, C. Horng, and K. Ju, J. Appl. Phys. **87**, 3415 (2000).
[33] D.T. Dekadjevi, P.A. Ryan, B.J. Hickey, B.D. Fulthorpe, and B.K. Tanner, Phys. Rev. Lett. **86**, 5787 (2001).
[34] J. Chen and J. Fernandez-de-Castro, J. Appl. Phys. **89**, 6934 (2001).
[35] W.H. Butler, X.-G. Zhang, T.C. Schulthess, D.M.C. Nicholson, A.B. Oparin, and J.M. MacLaren, J. Appl. Phys. **85**, 5834 (1999).
[36] C. Blaas, L. Szunyogh, P. Weinberger, C. Sommers, P.M. Levy, and J. Shi, Phys. Rev. B **65**, 134427 (2002).
[37] R. Kubo, J. Phys. Soc. Jpn. **12**, 570 (1957).
[38] M.R. Gibbons, M. Mao, and C. Chien, J. Appl. Phys. **89**, 6949 (2001).
[39] W.C. Uhlig, M. Mao, V. Yiu, J. Li, and J. Shi, J. Appl. Phys. **89**, 6937 (2001).
[40] Z.Q. Lu, G. Pan, A.A. Jibouri, and Y.K. Zheng, J. Appl. Phys. **91**, 287 (2002).
[41] J. Hong, J. Kane, J. Hashimoto, M. Yamagishi, K. Noma, and H. Kanai, IEEE Trans. Magn. **38**, 15 (2002).
[42] K. Nagasaka, Y. Seyama, L. Varga, Y. Shimizu, and A. Tanaka, J. Appl. Phys. **89**, 6943 (2001).
[43] J.M. De Teresa, A. Barthélémy, A. Fert, J.P. Contour, F. Montaigne, and P. Seneor, Science **286**, 507 (1999).
[44] S.B. Soffer, J. Appl. Phys. **38**, 1710 (1967).
[45] R. Lenk and A. Knäbchen, J. Phys.: Condens. Matter **5**, 6563 (1993).
[46] X.-G. Zhang and W.H. Butler, Phys. Rev. B **51**, 10 085 (1995).
[47] H.E. Camblong and P.M. Levy, Phys. Rev. Lett. **69**, 2835 (1992).
[48] R.Q. Hood, L.M. Falicov, and D.R. Penn, Phys. Rev. B **49**, 368 (1994).

[49] L. Wang, W.J. McMahon, B. Liu, Y.H. Wu, and C.T. Chong, Phys. Rev. B **69**, 214403 (2004).
[50] Th.G.S.M. Rijks, R. Coehoorn, M.J.M. de Jong, and W.J.M. de Jonge, Phys. Rev. B **51**, 283 (1995).
[51] H.J.M. Swagten, G.J. Strijkers, R.H.J.N. Bitter, W.J.M. de Jonge, and J.C.S. Kools, IEEE Trans. Magn. **34**, 948 (1998).
[52] B. Dieny, J. Phys.: Condens. Matter **4**, 8009 (1992).
[53] B. Dieny, Europhys. Lett. **17**, 261 (1992).
[54] W.E. Bailey, Ph.D. thesis, Stanford University, 2000.
[55] B. Dieny, P. Humbert, V.S. Speriosu, S. Metin, B.A. Gurney, P. Baumgart, and H. Lefakis, Phys. Rev. B **45**, 806 (1992).
[56] A. Barthélémy and A. Fert, Phys. Rev. B **43**, 13 124 (1991).
[57] M. Liu and D.Y. Xing, Phys. Rev. B **47**, 12 272 (1993).
[58] H.J.M. Swagten, M.M.H. Willekens, and W.J.M. De Jonge, in *Frontiers in Magnetism of Reduced Dimension Systems*, edited by V.G. Bar'yakthar, P.E. Wigen, and N.A. Lesnik (Kluwer Academic Publishers, Dordrecht, 1998), p. 471.
[59] B. Dieny, J. Magn. Magn. Mater. **136**, 335 (1994).
[60] C. Prados, D.V. Dimitrov, and G.C. Hadjipanayis, J. Magn. Magn. Mater. **192**, 19 (1999).
[61] C.H. Lai, C.J. Chen, and T.S. Chin, J. Appl. Phys. **89**, 6928 (2001).
[62] J.M. George, L.G. Pereira, A. Barthélémy, F. Petroff, L. Steren, J.L. Duvail, A. Fert, R. Loloee, P. Holody, and P.A. Schroeder, Phys. Rev. Lett. **72**, 408 (1994).
[63] N.F. Mott, Proc. R. Soc. London, Ser. A **156**, 368 (1936).
[64] J.E. Pask, L.H. Yang, C.Y. Fong, W.E. Pickett, and S. Dag, Phys. Rev. B **67**, 224420 (2003).
[65] H.J. Juretschke, J. Appl. Phys. **37**, 435 (1966).
[66] W.H. Butler, X.-G. Zhang, D.M.C. Nicholson, T.C. Schulthess, and J.M. MacLaren, Phys. Rev. Lett. **76**, 3216 (1996).
[67] K. Yamada, W.E. Bailey, C. Féry, and S.X. Wang, IEEE Trans. Magn. **35**, 2979 (1999).
[68] K.R. Coffey, B.A. Gurney, D.E. Heim, H. Lefakis, D. Mauri, V.S. Speriosu, and D. R. Wilhoit, U.S. Patent No. 5,583,725 (December 10, 1996).
[69] Z.Y. Zhang, Y.C. Feng, T. Clinton, G. Badran, N.H. Yeh, G. Tarnopolsky, E. Girt, M. Munteanu, S. Harkness, H. Richter, T. Nolan, R. Ranjan, S. Hwang, G. Rauch, M. Ghaly, D. Larson, E. Singleton, V. Vas'ko, J. Ho, F. Stageberg, V. Kong, K. Duxstad, and S. Slade, IEEE Trans. Magn. **38**, 1861 (2002).
[70] K. Stoev, F. Liu, Y. Chen, X. Dang, P. Luo, J. Chen, J. Wang, K. Kung, M. Lederman, M. Re, G. Choe, J.N. Zhou, and M. Yu, J. Appl. Phys. **93**, 6552 (2003).
[71] J. Chen, S.N. Mao, J. Fernandez-de-Castro, T.S. Choy, and S. Hershfield, IEEE Trans. Magn. **36**, 2885 (2000).
[72] Z.Q. Lu, G.H. Pan, A. Al-Jibouri, and M. Hoban, J. Appl. Phys. **91**, 7116 (2002).
[73] P.M. Baumgart, B. Dieny, B.A. Gurney, J.P. Nozieres, V.S. Speriosu, and D.R. Wilhoit, U.S. patent No. 5,287,238 (February 15, 1994).
[74] T.C. Anthony, J.A. Brug, and S.F. Zhang, IEEE Trans. Magn. **30**, 3819 (1994).
[75] W.F. Egelhoff, Jr., P.J. Chen, C.J. Powell, M.D. Stiles, R.D. McMichael, C.-L. Lin, J.M. Sivertsen, J.H. Judy, K. Takano, and A.E. Berkowitz, J. Appl. Phys. **79**, 8603 (1996).
[76] M.J. Carey, T. Le, T. Thompson, and B.A. Gurney, J. Appl. Phys. **92**, 4538 (2002).